

Global Regulation and Excitation via Attention Tuning for Stereo Matching

Jiahao LI¹ Xinhong Chen¹ Zhengmin JIANG¹

¹City University of Hong Kong

Qian Zhou¹ Yung-Hui Li²

²Hon Hai Research Institute

jiahali2-c@my.cityu.edu.hk

Abstract

Stereo matching achieves significant progress with iterative algorithms like RAFT-Stereo and IGEV-Stereo. However, these methods struggle in ill-posed regions with occlusions, textureless, or repetitive patterns, due to a lack of global context and geometric information for effective iterative refinement. To enable the existing iterative approaches to incorporate global context, we propose the Global Regulation and Excitation via Attention Tuning (GREAT) framework which encompasses three attention modules. Specifically, Spatial Attention (SA) captures the global context within the spatial dimension, Matching Attention (MA) extracts global context along epipolar lines, and Volume Attention (VA) works in conjunction with SA and MA to construct a more robust cost-volume excited by global context and geometric details. To verify the universality and effectiveness of this framework, we integrate it into several representative iterative stereo-matching methods and validate it through extensive experiments, collectively denoted as GREAT-Stereo. This framework demonstrates superior performance in challenging ill-posed regions. Applied to IGEV-Stereo, among all published methods, our GREAT-IGEV ranks first on the Scene Flow test set, KITTI 2015, and ETH3D leaderboards, and achieves second on the Middlebury benchmark. Code is available at <https://github.com/JarvisLee0423/GREAT-Stereo>.

1. Introduction

Recovering depth information from 2D images is vital in 3D scene reconstruction which improves scene perception in fields like robotics and autonomous driving. Stereo matching intends to predict dense 3D representations referred to as disparity. This technique constructs the pixel-wise cost volume from rectified stereo images to depict matching similarity along epipolar lines and regresses disparity by refining cost volume [13].

Taking advantage of deep learning, the current state-of-the-art stereo-matching algorithms are primarily categorized as aggregation-based and iteration-based approaches.

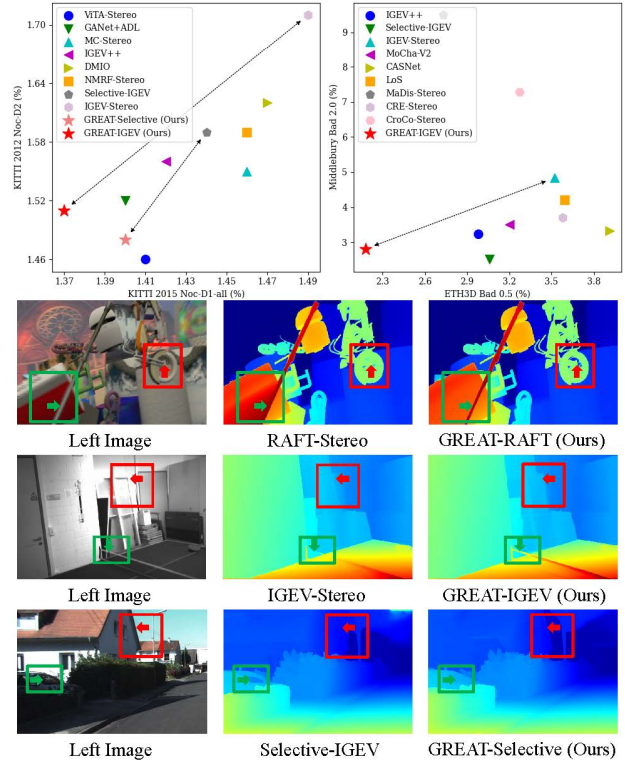


Figure 1. **Row 1:** Comparisons with state-of-the-art stereo methods on KITTI 2012 [10], KITTI 2015 [26], ETH3D [29], and Middlebury [28] leaderboards, where the lower metrics indicate better performance. **Row 2:** Visual comparison with RAFT-Stereo on Scene Flow [25]. **Row 3:** Visual comparison with IGEV-Stereo on ETH3D. **Row 4:** Visual comparison with Selective-IGEV on KITTI 2012. Our models produce clearer and more consistent geometric structures in ill-posed regions (green and red boxes).

Aggregation-based methods [5, 12, 16, 38, 39, 41, 42, 44] leverage convolutional neural network (CNN) to aggregate geometric structures within the pixel-wise cost volume to predict disparity. While these methods achieve superior accuracy, the substantial computational cost makes them impractical for high-resolution images. To address this limitation, researchers turn to iterative schemes [17, 18, 51], which avoid computationally expensive cost-volume aggre-

gation. Specifically, these methods employ recurrent units [18] to progressively update the disparity based on local information retrieved from the pixel-wise cost volume, allowing for high-resolution inference.

Despite these advancements, iterative methods still encounter challenges in ambiguous ill-posed regions (occluded, textureless, and repetitive texture areas) due to merely considering pixel-wise and local contextual details. Specifically, the CNN feature extractors widely adopted by iterative approaches use a fixed receptive field size, restricting each pixel feature to encode only local context with its nearest neighboring pixels. Meanwhile, iterative methods rely on a cost-volume constructed on a pixel-by-pixel basis to compute matching similarity [18, 51, 55], thereby the points in ill-posed regions like textureless and repetitive areas with similar local features cannot be effectively distinguished and matched [43]. Moreover, the recurrent units adopted by iterative schemes cannot effectively refine the geometry in disparity based on limited local information in each pixel [37], resulting in blurry geometric structures of different objects and incorrect matching between images.

Based on the above observations, the key to improving the stereo-matching performance of iterative methods in ill-posed regions is to introduce global context information. Specifically, for occluded areas, the complementary information from the global context beyond local neighborhoods can help propagate the geometric structures from non-occluded to occluded regions and yield reliable predictions in occlusions, as demonstrated in GMA-Flow [14]. As for textureless and repetitive texture regions, although these areas are challenging to distinguish at the pixel or local level due to similar patterns, assigning them to the correct geometric structures becomes feasible when the receptive fields are expanded to encompass the global context. Therefore, in this work, we propose to enable the existing iterative methods to incorporate global context details so that they can robustly handle the matching ambiguities in ill-posed regions.

To this end, we introduce a universal framework called **Global Regulation and Excitation via Attention Tuning** (GREAT) that contains three attention modules. **Spatial Attention** (SA) encodes global context in spatial dimension from local to global into each pixel, accelerating the propagation of geometric structures within the cost volume. **Matching Attention** (MA) aggregates global context for each pixel along epipolar lines, effectively reducing ambiguities in pixel pair matching. **Volume Attention** (VA) excites global context in specific regions of the cost volume by incorporating SA and MA, enhancing its robustness. Based on these modules, as illustrated in Fig. 1, the proposed framework—**GREAT-Stereo** produces clearer and more consistent geometric structures in ill-posed regions compared to baseline by leveraging global context details, thereby enhancing the accuracy in such regions. We vali-

date the effectiveness of our framework in several experiments. When applied to IGEV-Stereo [43], on the Scene Flow dataset, our GREAT-IGEV achieves the new state-of-the-art overall EPE of 0.41 and non-occluded EPE of 0.14. Compared to the state-of-the-art occluded EPE of 1.53 in GOAT-Stereo [23], our GREAT-IGEV obtains an even lower occluded EPE of 1.51 and eliminates the need for yielding an additional occlusion mask. Meanwhile, among all published methods, our GREAT-IGEV ranks first on both KITTI 2015 [26] and ETH3D [29] leaderboards and achieves second on Middlebury [28] benchmark. Our main contributions can be summarized as follows:

- We propose a universal framework that can be integrated into existing iterative stereo-matching methods to improve the performance in ill-posed regions.
- We introduce Spatial (SA), Matching (MA), and Volume (VA) Attentions, designed to mitigate ambiguities in ill-posed regions with global context information.
- Our method outperforms existing published methods on public leaderboards such as SceneFlow, KITTI, ETH3D, and Middlebury, with especially significant improvements in ill-posed regions.

2. Related Work

Aggregation-based & Iterative Approaches. Thanks to deep learning, there has been a proliferation of neural network architectures for stereo matching [5–7, 12, 16, 31, 40, 42, 44, 46, 52, 54]. Methods such as DispNet [25], GCNet [16], PSMNet [5], and ACVNet [42], compute a pixel-wise cost volume and deploy 3D CNN to aggregate it for disparity prediction. However, the high computational demands of 3D CNN limit their efficiency, especially in high-resolution images. To address this, cascaded methods [11, 30, 44] have been introduced, which employ a coarse-to-fine strategy to improve efficiency, albeit propagating coarse disparity errors. In response, iterative methods [17, 18, 37, 43, 45, 51, 55] have been proposed, such as RAFT-Stereo [18] which recurrently updates the disparity using local correlation information retrieved from the cost volume and IGEV-Stereo [43] that integrates aggregation and iterative mechanisms with a lightweight 3D CNN to capture non-local geometric structures. These iterative schemes stand out for balancing computational efficiency and performance.

Ill-posed Ambiguities in Stereo Matching. Despite the observed advancements [5, 18, 25, 42, 43], the ill-posed ambiguities in stereo matching continue to pose a challenge. To combat this issue, researchers have introduced uncertainty-guided approaches [15, 19, 23, 35, 55], aimed at improving performance in occluded areas. UGAW-Stereo [15] generates an uncertainty map to guide the construction of the cost volume. Similarly, GOAT-Stereo [23] and ER-CNet [19] use uncertainty maps as error indicators to help

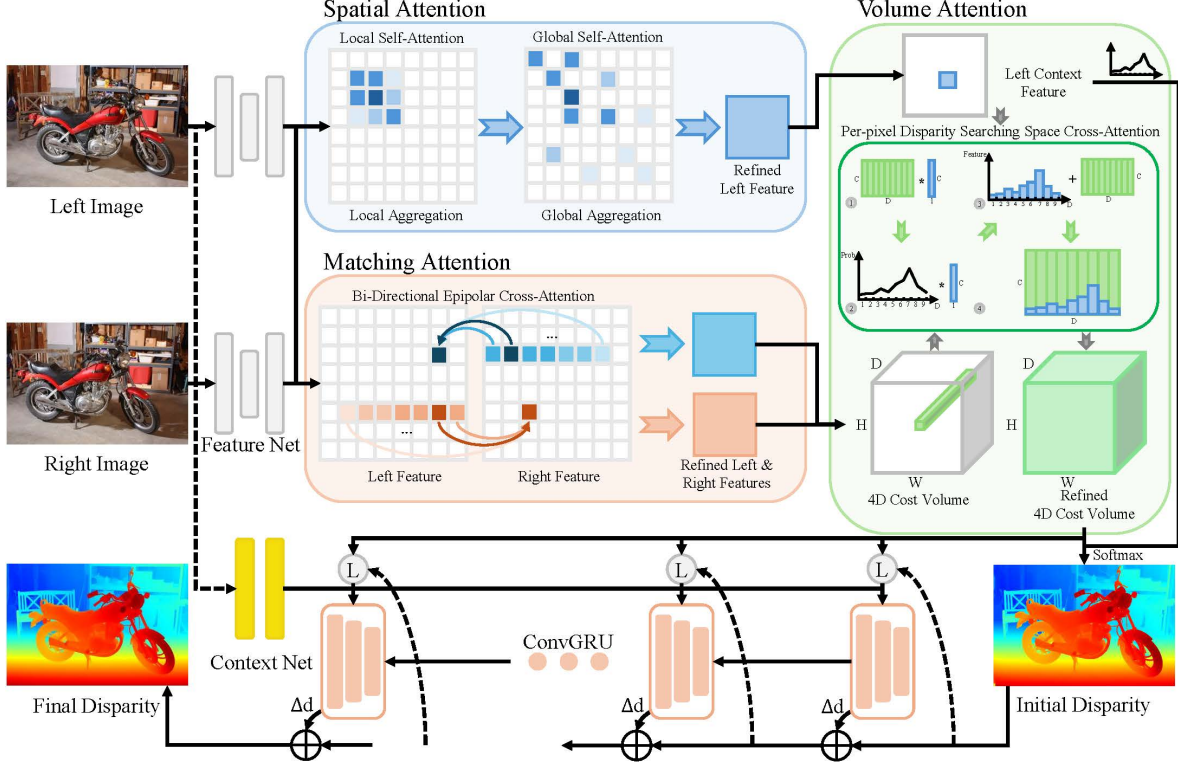


Figure 2. Overview of our proposed GREAT-Stereo (GREAT-IGEV version). The GREAT-Stereo first constructs the cost volume with Matching Attention (MA) which encodes global context along epipolar lines in left and right features. Then, Spatial Attention (SA) extracts global context information from the spatial dimension of left feature and incorporates with Volume Attention (VA) to further involve global geometry in the cost volume which is used to generate an initialized disparity map and participate in iterations of ConvGRU.

identify occlusions and deploy left images to enhance areas characterized by high uncertainty. However, while these uncertainty-guided techniques provide improvements, they do not fully uncover the underlying causes of matching ambiguities in ill-posed regions. GMA-Flow [14] is one of the pioneers that explore the principles behind these ambiguities, noting that global motion can be utilized to propagate information from non-occluded to occluded regions, thereby supporting more reliable predictions in such areas. Analogously, IGEV-Stereo [43] and Selective-Stereo [37] suggest that leveraging non-local geometric cues and varying receptive fields can yield robust results for textureless and repetitive texture regions. On top of these findings, our proposed GREAT-Stereo framework extracts global context information from both spatial dimension and epipolar lines to construct a more robust cost volume for stereo matching, which has achieved outstanding performance in tackling ill-posed regions, such as occluded, textureless, and repetitive texture areas.

3. Method

In this section, we introduce the GREAT-Stereo, a universal framework designed to improve the performance of various

iterative stereo-matching methods in ill-posed regions. We present GREAT-IGEV (Fig. 2) as an example and focus on illustrating its key components.

3.1. Framework Outline

For fair comparisons, GREAT-IGEV maintains consistency with IGEV-Stereo [43] by employing MobileNetV2 [27] for the extraction of multi-scale left and right features $\mathbf{f}_{l(r),i} \in \mathbb{R}^{C_i \times \frac{H}{i} \times \frac{W}{i}}$ ($i = 4, 8, 16, 32$ and C_i for feature channels) from stereo images $\mathbf{I}_{l(r)} \in \mathbb{R}^{3 \times H \times W}$. Taking the left features $\mathbf{f}_{l,i}$ ($i = 4, 8, 16, 32$) as input, **Spatial Attention** (SA in Sec. 3.2) aggregates context details in a local-to-global fashion. Concurrently, **Matching Attention** (MA in Sec. 3.3) captures detailed global context along epipolar lines using the largest-scale left and right features $\mathbf{f}_{l(r),4}$, facilitating the construction of a concatenation-based cost volume \mathbf{C}_{cat} . This cost volume is refined by **Volume Attention** (VA in Sec. 3.4), which incorporates insights gained from the SA, resulting in a robust cost volume that leads to accurate initial disparity. In line with IGEV-Stereo, the same local correlation sampler [43] is utilized to retrieve information from \mathbf{C}_{cat} , which is then integrated with ConvGRU [18, 43] to iteratively predict the final disparity.

3.2. Spatial Global Context Aggregation

To facilitate the propagation of geometric structures in occlusions, the **Spatial Attention** (SA) captures richer contextual details from multi-scale left features $\mathbf{f}_{l,i}$ ($i = 4, 8, 16, 32$) in a local-to-global fashion by leveraging attention mechanism [9, 34]. This is accomplished through two attention mechanisms applied to each scale individually: Local Self-Attention (LSA) originated from Vision-Outlooker [50] and Global Self-Attention (GSA) derived from Swin-Transformer [22], as depicted in Fig. 2.

Local Self-Attention. With inputs $\mathbf{f}_{l,i}$ ($i = 4, 8, 16, 32$), LSA compensates for local geometry and generates multi-scale local geometric left features $\mathbf{f}_{l,i}^{local} \in \mathbb{R}^{C_i \times \frac{H}{t} \times \frac{W}{t}}$ ($i = 4, 8, 16, 32$) using Outlook Attention [50], formulated as:

$$\begin{aligned}\mathbf{f}_{l,i}^{local} &= \text{OutlookAttn}(\text{LN}(\mathbf{f}_{l,i})) + \mathbf{f}_{l,i} \\ \mathbf{f}_{l,i}^{local} &= \text{MLP}(\text{LN}(\mathbf{f}_{l,i}^{local})) + \mathbf{f}_{l,i}^{local}\end{aligned}\quad (1)$$

where LN stands for LayerNorm [21] and MLP refers to a multilayer perceptron. Outlook Attention employs a $K \times K$ window centered at each spatial location (m, n) within $\mathbf{f}_{l,i}$ and involves three linear projections: *to_attn* computes the attention weights $\mathbf{W}_A^{outlook} \in \mathbb{R}^{K^2}$ from vector $\mathbf{v}_{l,i} \in \mathbb{R}^{C_i}$ at location (m, n) ; *to_value* generates value features $\mathbf{W}_V^{outlook} \in \mathbb{R}^{C_i \times K^2}$ from assigned windows; and *to_out* aggregates final vector $\mathbf{v}_{l,i}^{local} \in \mathbb{R}^{C_i}$ at location (m, n) by multiplying the softmax of $\mathbf{W}_A^{outlook}$ and $\mathbf{W}_V^{outlook}$ as follows:

$$\begin{aligned}\mathbf{v}_{l,i}^{local} &= \sum_{k=1}^{K^2} \text{Softmax}(\mathbf{W}_A^{outlook}) \cdot \mathbf{W}_V^{outlook} \\ \mathbf{v}_{l,i}^{local} &= \text{to_out}(\mathbf{v}_{l,i}^{local})\end{aligned}\quad (2)$$

Global Self-Attention. Utilizing $\mathbf{f}_{l,i}^{local}$ ($i = 4, 8, 16, 32$) from LSA, GSA encodes global geometry across the entire spatial dimension, producing multi-scale global geometric left features $\mathbf{f}_{l,i}^{spatial} \in \mathbb{R}^{C_i \times \frac{H}{t} \times \frac{W}{t}}$ ($i = 4, 8, 16, 32$). To address the high computational cost of full spatial dimensions ($\mathbf{H} \times \mathbf{W}$), Window Attention from Swin-Transformer [22] has been implemented as follows:

$$\begin{aligned}\mathbf{f}_{l,i}^{local} &= \text{PE}(\mathbf{f}_{l,i}^{local}) + \mathbf{f}_{l,i}^{local} \\ \mathbf{f}_{l,i}^{spatial} &= \text{WSA}(\text{LN}(\mathbf{f}_{l,i}^{local})) + \mathbf{f}_{l,i}^{local} \\ \mathbf{f}_{l,i}^{spatial} &= \text{MLP}(\text{LN}(\mathbf{f}_{l,i}^{spatial})) + \mathbf{f}_{l,i}^{spatial} \\ \mathbf{f}_{l,i}^{spatial} &= \text{SWSA}(\text{LN}(\mathbf{f}_{l,i}^{spatial})) + \mathbf{f}_{l,i}^{spatial} \\ \mathbf{f}_{l,i}^{spatial} &= \text{MLP}(\text{LN}(\mathbf{f}_{l,i}^{spatial})) + \mathbf{f}_{l,i}^{spatial}\end{aligned}\quad (3)$$

where PE denotes positional embedding [9, 34], while WSA and SWSA are Window Self-Attention and Shifted-Window Self-Attention, respectively. WSA divides the

whole spatial dimension into k windows of size $\frac{H}{k} \times \frac{W}{k}$, reducing memory cost by calculating attention within each window. To ensure completed global aggregation, SWSA computes the attention map inside shifted windows by rolling it from left-to-right and up-to-down with strides of $\frac{W}{2k}$ and $\frac{H}{2k}$, respectively.

3.3. Bi-Directional Epipolar Global Refinement

To mitigate the matching ambiguities in textureless and repetitive texture regions, **Matching Attention** (MA) captures global context along epipolar lines using both largest-scale of left $\mathbf{f}_{l,4}$ and right $\mathbf{f}_{r,4}$ features. This is achieved via Bi-Directional Epipolar Cross-Attention (BECA), which utilizes one-dimensional attention, as illustrated in Fig. 2.

Mitigation of Imperfective Rectification. The BECA enhances global matching along epipolar lines using both left $\mathbf{f}_{l,4}$ and right $\mathbf{f}_{r,4}$ features, increasing sensitivity to rectification imperfections. Consequently, non-parallel epipolar lines may introduce additional noise post-BECA. To mitigate this, a streamlined pipeline encodes information from varying receptive fields around the epipolar lines using the Contextual Spatial Attention Module in Selective-Stereo [37]. Specifically, two CNNs with small (kernel = 3) and large (kernel = 5) receptive fields aggregate different frequency information from $\mathbf{f}_{l,4}$ and $\mathbf{f}_{r,4}$. Then an attention map from [37] fuses these features ($\mathbf{f}_{l(r),4}^{fused} \in \mathbb{R}^{C_4 \times \frac{H}{4} \times \frac{W}{4}}$), encoding more local geometry around the epipolar lines and thereby enhancing robustness to imperfect rectification.

Bi-Directional Epipolar Cross Attention. Given the fused features $\mathbf{f}_{l,4}^{fused}$ and $\mathbf{f}_{r,4}^{fused}$ derived from stereo images \mathbf{I}_l and \mathbf{I}_r , BECA produces matching left and right features ($\mathbf{f}_{l(r),4}^{mat} \in \mathbb{R}^{C_4 \times \frac{H}{4} \times \frac{W}{4}}$) for constructing a robust cost volume. To expedite bi-directional cross-attention from left to right and vice versa, these feature maps are first concatenated along the batch dimension, formulated as follows:

$$\begin{aligned}\mathbf{f}_{l \rightarrow r,4}^{cat} &= \langle \mathbf{f}_{l,4}^{fused} \mid \mathbf{f}_{r,4}^{fused} \rangle \\ \mathbf{f}_{r \rightarrow l,4}^{cat} &= \langle \mathbf{f}_{r,4}^{fused} \mid \mathbf{f}_{l,4}^{fused} \rangle\end{aligned}\quad (4)$$

where $\langle A \mid B \rangle$ denotes concatenation between features A and B , yielding $\mathbf{f}_{*,4}^{cat} \in \mathbb{R}^{2 \times C_4 \times \frac{H}{4} \times \frac{W}{4}}$ with $*$ refers to $l \rightarrow r$ or $r \rightarrow l$. Subsequently, one-dimensional cross-attention is applied along the width to generate an attention map of shape $\frac{W}{4} \times \frac{W}{4}$, aggregating global context along epipolar lines, defined as follows:

$$\begin{aligned}\mathbf{f}_{*,4}^{cat} &= \text{LN}(\text{PE}(\mathbf{f}_{*,4}^{cat}) + \mathbf{f}_{*,4}^{cat}) \\ \mathbf{f}_{l \rightarrow r,4}^{cat} &= \text{CrossAttn}(\mathbf{f}_{l \rightarrow r,4}^{cat}, \mathbf{f}_{r \rightarrow l,4}^{cat}) + \mathbf{f}_{l \rightarrow r,4}^{cat} \\ \mathbf{f}_{l \rightarrow r,4}^{cat} &= \text{MLP}(\text{LN}(\mathbf{f}_{l \rightarrow r,4}^{cat})) + \mathbf{f}_{l \rightarrow r,4}^{cat}\end{aligned}\quad (5)$$

Finally, $\mathbf{f}_{l \rightarrow r,4}^{cat}$ is decomposed into $\mathbf{f}_{l,4}^{mat}$ and $\mathbf{f}_{r,4}^{mat}$ along batch axis for the subsequent processing.

3.4. Cost Volume Construction and Refinement

To directly introduce global context and geometric structures into cost volume, **Volume Attention** (VA) excites global context details from specific positions within cost volume by leveraging the spatial features $\mathbf{f}_{l,i}^{spatial}$ ($i = 4, 8, 16, 32$) derived from Spatial Attention (Sec. 3.2).

Concatenated Cost Volume. To accurately identify positions that require global context excitation within the cost volume, it is essential to ensure consistency in feature distribution between $\mathbf{f}_{l,i}^{spatial}$ and cost volume. Consequently, the cost volume \mathbf{C}_{cat} is constructed by concatenating matching features $\mathbf{f}_{l(r),4}^{mat}$ from Matching Attention (Sec. 3.3) along the channel dimension, rather than computing correlations between them, formulated as follows:

$$\mathbf{C}_{cat}(\cdot, d, x, y) = \langle \mathbf{f}_{l,4}^{mat}(x, y) | \mathbf{f}_{r,4}^{mat}(x-d, y) \rangle \quad (6)$$

where $\mathbf{C}_{cat} \in \mathbb{R}^{C_4 \times D \times \frac{H}{4} \times \frac{W}{4}}$ denotes the 4D concatenated cost volume, with $d \in \{0, 1, \dots, D-1\}$ referring the d^{th} disparity searching space. We also calculate all-pairs correlations [18] to ensure consistency with IGEV-Stereo.

Per-pixel Disparity Searching Space Cross-Attention.

The core technique of VA, Per-pixel Disparity Searching Space Cross-Attention (PDCA), is integrated into each scale of the UNet in [43], replacing the Feature Attention from [1]. As shown in Fig. 2, PDCA employs a soft-classification scheme to identify positions in cost volume that require global context enhancement through per-pixel cross-attention, defined as follows:

$$\begin{aligned} \mathbf{A}_{m,n} &= \text{Softmax}(\mathbf{M}_{m,n}^C \cdot \mathbf{v}_{m,n}^f) \\ \mathbf{M}_{m,n}^C &= \text{MLP}(\mathbf{A}_{m,n} \cdot \mathbf{v}_{m,n}^f) + \mathbf{M}_{m,n}^C \end{aligned} \quad (7)$$

where $\mathbf{M}_{m,n}^C \in \mathbb{R}^{C_4 \times D}$ represents the disparity searching space matrix at pixel location (m, n) in \mathbf{C}_{cat} , $\mathbf{v}_{m,n}^f \in \mathbb{R}^{C_4}$ is the spatial feature vector at the same location in $\mathbf{f}_{l,i}^{spatial}$, and $\mathbf{A}_{m,n} \in \mathbb{R}^D$ denotes the attention map specifying the enhancement proportion in the disparity searching space. This formulation enables PDCA to directly excite global context in specific positions within the cost volume by referring to spatial features, instead of solely filtering the distribution like in Feature Attention [1].

3.5. Loss Function

Aligned with IGEV-Stereo [43], the initial disparity \mathbf{d}_0 regressed from \mathbf{C}_{cat} is supervised by Smooth L1 loss [5], while an L1 loss with exponentially increasing weights [18] is applied to all updated disparities $\{\mathbf{d}_i\}_{i=1}^N$. The total loss is defined as follows:

$$\begin{aligned} \mathcal{L}_{init} &= \text{SmoothL}_1(\mathbf{d}_0 - \mathbf{d}_{gt}) \\ \mathcal{L}_{stereo} &= \mathcal{L}_{init} + \sum_{i=1}^N \gamma^{N-i} \|\mathbf{d}_i - \mathbf{d}_{gt}\|_1 \end{aligned} \quad (8)$$

where \mathbf{d}_{gt} denotes the ground truth disparity and $\gamma = 0.9$.

4. Experiments

In this section, we conduct extensive experiments and ablation studies to validate the effectiveness and universality of our proposed GREAT-Stereo framework.

4.1. Datasets

Scene Flow [25], a synthetic dataset, includes 35454 training and 4370 testing pairs with dense disparity maps. We utilize the finalpass version for its more realistic and challenging characteristics over the cleanpass version. **KITTI 2012** [10] and **KITTI 2015** [26] provide real-world driving scene data. KITTI 2012 offers 194 training and 195 testing pairs, and KITTI 2015 supplies 200 training and 200 testing pairs. **ETH3D** [29] includes 27 training and 20 testing gray-scale stereo pairs for both indoor and outdoor scenarios. **Middlebury** [28] known as high-resolution indoor scenes, comprises 15 training and 15 testing pairs.

4.2. Implementation Details

We implement GREAT-Stereo with PyTorch and train the models on NVIDIA RTX 3090 and 4090 GPUs. For all experiments, we use the AdamW [24] optimizer with gradient clipping set to $[-1, 1]$ and the one-cycle [32] learning rate schedule with a learning rate of $2e-4$. Pretraining is conducted on the Scene Flow dataset for 200k steps with a batch size of 8. During pretraining, the image crops are 320 x 720 for models based on RAFT-Stereo [18] and 320 x 736 for models based on IGEV-Stereo [43], and the number of iterations is set to 22. For the number of attention blocks, each scale applies only one Spatial Attention and one Volume Attention block. Concurrently, the largest scale utilizes four Matching Attention blocks.

4.3. Ablation Study

In this section, we evaluate multiple variants of our framework to verify the proposed modules in several aspects. All results use 32 update iterations.

Effectiveness of Proposed Modules. To assess the proposed framework, we take IGEV-Stereo [43] as the baseline, integrating Spatial (SA), Matching (MA), and Volume (VA) Attentions. As shown in Tab. 1, VA universally improves accuracy, even without global context aggregation via SA and MA. This suggests that proactively exciting geometric details by spatial features creates a more robust cost volume. In Tab. 1, SA effectively propagates non-occluded information to occluded regions by incorporating global context, thereby enhancing occlusion handling. Additionally, MA enriches global context along epipolar lines, aiding in the disambiguation of textureless or repetitive texture areas (see Fig. 3), optimizing non-occluded regions. Consequently, SA and MA enhance the performance of VA, highlighting the effectiveness of the proposed framework in addressing ill-posed issues by enriching the global context.

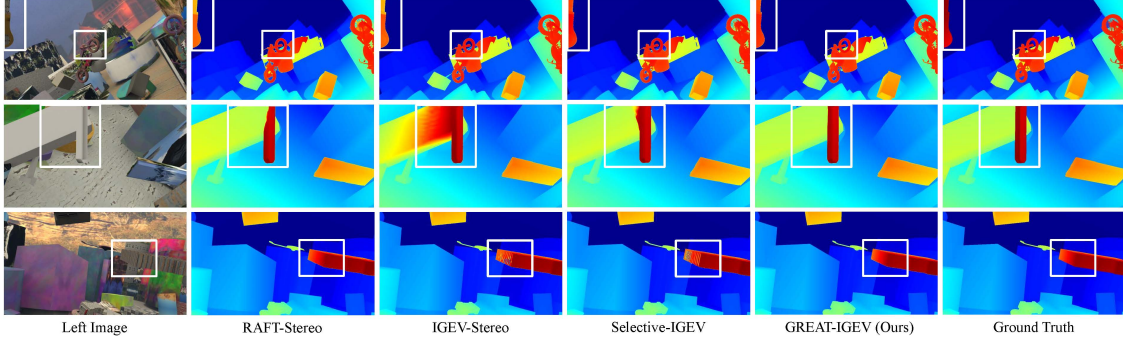


Figure 3. Qualitative results on the Scene Flow test set. Our GREAT-IGEV outperforms other iterative methods in occluded (**Row 1**), textureless (**Row 2**), and repetitive texture (**Row 3**) regions.

Model	Corr	VA	SA	MA	All		Non-Occ		Occ		Param (M)
					EPE (px)	D3 (%)	EPE (px)	D3 (%)	EPE (px)	D3 (%)	
Baseline (IGEV-Stereo)	✓				0.479	2.476	0.194	0.633	1.649	10.980	12.60
C_{corr} + Volume	✓	✓			0.469	2.443	0.187	0.621	1.623	10.914	12.91
C_{cat} + Volume		✓			0.466	2.437	0.183	0.612	1.616	10.860	12.91
C_{cat} + Volume + Spatial	✓	✓			0.457	2.418	0.181	0.623	1.587	10.698	13.62
C_{cat} + Matching			✓		0.430	2.229	0.153	0.483	1.558	10.283	13.40
Full Model (GREAT-IGEV)	✓	✓	✓		0.413	2.201	0.135	0.486	1.514	10.115	14.44

Table 1. Ablation study of the effectiveness of the proposed modules on the Scene Flow test set (**bold**: best). Corr denotes the correlation-based cost volume, Volume (VA) refers to Volume Attention, Spatial (SA) represents Spatial Attention, and Matching (MA) indicates Matching Attention. EPE means the End-Point Error to describe the overall errors. D3 signifies the proportion of pixels with errors exceeding 3 px. All, Non-Occ, and Occ respectively denote the entire, non-occluded, and occluded regions.

Model	All	Non-Occ	Occ	Param (M)
RAFT-Stereo [18]	0.551	0.214	1.938	11.12
GREAT-RAFT	0.488	0.183	1.747	12.40
IGEV-Stereo [43]	0.479	0.194	1.649	12.60
GREAT-IGEV	0.413	0.135	1.514	14.44
Selective-IGEV [37]	0.453	0.173	1.574	13.14
GREAT-Selective	0.419	0.146	1.524	14.98

Table 2. Ablation study of the cross-model transferability of the proposed framework (**bold**: best). Results report the End-Point Error (EPE) in corresponding regions on the Scene Flow test set.

Cross-Model Transferability of Proposed Modules.

To evaluate the universality of the proposed GREAT-Stereo framework, we integrate SA, MA, and VA into three baselines: RAFT-Stereo [18], IGEV-Stereo [43], and Selective-IGEV [37]. The resulting models are denoted as GREAT-RAFT, GREAT-IGEV, and GREAT-Selective. Particularly, RAFT-Stereo includes only all-pairs correlation and lacks multi-scale spatial features, thus, only MA is integrated to ensure minimal modification and fair comparison. As shown in Tab. 2, integrating these attention mechanisms significantly improves EPE metrics across all regions, including ill-posed areas, on the Scene Flow test set. Notably, incorporating only MA optimizes the EPE of RAFT-Stereo in occlusions by 9.9%. When using the full framework, GREAT-IGEV and GREAT-Selective reduce EPE in

Model	Number of Iterations					
	1	2	4	8	16	32
RAFT-Stereo [18]	2.053	1.134	0.754	0.596	0.554	0.551
GREAT-RAFT	1.646	0.950	0.664	0.530	0.492	0.488
IGEV-Stereo [43]	0.669	0.623	0.557	0.504	0.483	0.479
GREAT-IGEV	0.572	0.535	0.483	0.439	0.417	0.413

Table 3. Ablation study of the number of iterations (**bold**: best). Results report the EPE on the Scene Flow test set.

occlusions by 8.2% and 3.2%, respectively. As illustrated in Fig. 1 and 3, the integration of SA, MA, and VA significantly improves performance in textureless and repetitive texture regions, enabling GREAT-IGEV and GREAT-Selective to achieve even greater optimizations of 30.4% and 15.6% in non-occluded EPE, respectively. In summary, our framework can be seamlessly integrated into various stereo matching methods, significantly enhancing their performance in ill-posed regions.

Number of Iterations. Our GREAT-Stereo achieves comparable or better performance with fewer iterations. As shown in Tab. 3, GREAT-IGEV matches the performance of IGEV-Stereo [43] with only 4 iterations. This shows our framework optimizes ill-posed regions and boosts iterative methods' overall performance via a global-context-enhanced robust cost volume, thereby obtaining comparable performance with only a quarter of the iterations.

Metrics	GANet [52]	LEA-Stereo [8]	ACVNet [42]	GOAT-Stereo [23]	RAFT-Stereo [18]	IGEV-Stereo [43]	Selective-IGEV [37]	GREAT-IGEV (Ours)
EPE-Non-Occ (px)	-	-	-	-	0.21	0.19	0.17	0.14
EPE-Occ (px)	-	-	-	1.53	1.94	1.65	1.57	1.51
EPE-All (px)	0.84	0.78	0.48	0.47	0.55	0.48	0.45	0.41

Table 4. Quantitative evaluation on Scene Flow test set (**bold**: best).

Model	KITTI 2012				KITTI 2015				Param (M)
	2-noc	2-all	3-noc	3-all	D1-all	D1-fg	Noc-D1-all	Noc-D1-fg	
LEA-Stereo [8]	1.90	2.39	1.13	1.45	1.65	2.91	1.51	2.65	1.80
ACVNet [42]	1.83	2.35	1.13	1.47	1.65	3.07	1.52	2.84	6.20
ViTAStereo [20]	1.46	1.80	0.93	1.16	<u>1.50</u>	2.99	1.41	2.90	-
IGEV-Stereo [43]	1.71	2.17	1.12	1.44	1.59	2.67	1.49	2.62	12.60
Selective-IGEV [37]	1.59	2.05	1.07	1.38	1.55	2.61	1.44	2.55	13.14
IGEV++ [45]	1.56	2.03	1.04	1.36	1.51	2.54	1.42	2.54	14.53
GREAT-IGEV (Ours)	1.51	2.00	1.02	1.37	<u>1.50</u>	<u>2.59</u>	1.37	2.51	14.44
GREAT-Selective (Ours)	<u>1.48</u>	<u>1.94</u>	<u>1.00</u>	<u>1.31</u>	1.49	2.62	<u>1.40</u>	2.60	14.98

Table 5. Quantitative evaluation on KITTI 2012 and KITTI 2015 benchmarks (**bold**: best; underline: second best).

Model	KITTI 2015	Middlebury half	Middlebury quarter	ETH3D
HD3 [49]	26.5	37.9	20.3	54.2
GwCNet [12]	22.7	34.2	18.1	30.1
DSMNet [53]	6.5	13.8	8.1	6.2
RAFT-Stereo [18]	5.8	10.0	6.7	<u>3.2</u>
IGEV-Stereo [43]	6.0	9.5	6.2	3.6
Selective-IGEV [37]	6.1	9.2	6.6	5.4
GREAT-RAFT (Ours)	5.8	10.2	7.0	2.8
GREAT-IGEV (Ours)	<u>5.9</u>	<u>8.6</u>	<u>5.1</u>	3.8
GREAT-Selective (Ours)	6.2	8.1	<u>4.6</u>	3.7

Table 6. Zero-shot generalization of the proposed framework (**bold**: best; underline: second best). All models are trained on Scene Flow. The 3-pixel error rate is used for KITTI 2015, 2-pixel error rate for Middlebury, and 1-pixel error rate for ETH3D.

4.4. Zero-shot Generalization

Due to scarce large real-world training data, zero-shot generalization of stereo models is critical. To assess this and verify that baseline improvements do not stem from overfitting, we train the GREAT-RAFT/IGEV/Selective on synthetic Scene Flow [18] dataset, then test them on real-world KITTI 2015 [26], Middlebury [28], and ETH3D [29] training sets without fine-tuning. As shown in Tab. 6, our framework matches or outperforms in the same zero-shot setting.

4.5. Comparisons with State-of-the-art

All fine-tuned models are initialized with the pretrained Scene Flow model. Each target dataset uses distinct fine-tuning strategies. For validations, GREAT-RAFT is benchmarked against RAFT-Stereo [18], GREAT-IGEV against IGEV-Stereo [43], and GREAT-Selective against Selective-IGEV [37], using each respective model as the baseline.

Scene Flow. As shown in Tab. 2 and 4, our GREAT-IGEV model achieves a state-of-the-art overall EPE of

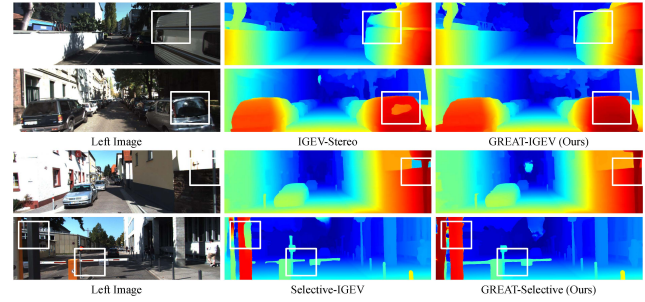


Figure 4. Qualitative results on the KITTI test set. **Rows 1 & 2** are the KITTI 2012, and **Rows 3 & 4** are the KITTI 2015.

0.413 on the Scene Flow test set, representing a 13.8% optimization over IGEV-Stereo [43] and a significant 47.4% better than LEA-Stereo [8]. Additionally, GREAT-Selective attains a comparable overall EPE of 0.419, surpassing Selective-IGEV [37] by 7.5%. To assess the performance of our model in ambiguous regions, we partition the Scene Flow test set into Non-Occluded and Occluded areas using a ground truth occlusion mask. As shown in Tab. 4, GREAT-IGEV outperforms IGEV-Stereo [43] by 8.2% on occluded EPE and achieves even lower occluded EPE of 1.51 compared to GOAT-Stereo [23] (1.53) which requires to predict an additional occlusion mask. As indicated in Tab. 1 and Fig. 3, GREAT-IGEV excels in textureless and repetitive texture areas, resulting in a 30.4% reduction on non-occluded EPE compared to IGEV-Stereo.

KITTI. Our model is first fine-tuned on VKITTI2 [4] for 60k steps, followed by further fine-tuning on a mixed dataset of KITTI 2012 and 2015 for 50k steps with a batch size of 8. As shown in Tab. 5, our models rank first on KITTI 2015 and second on KITTI 2012 among all published methods. On KITTI 2012, our GREAT-Selective sur-

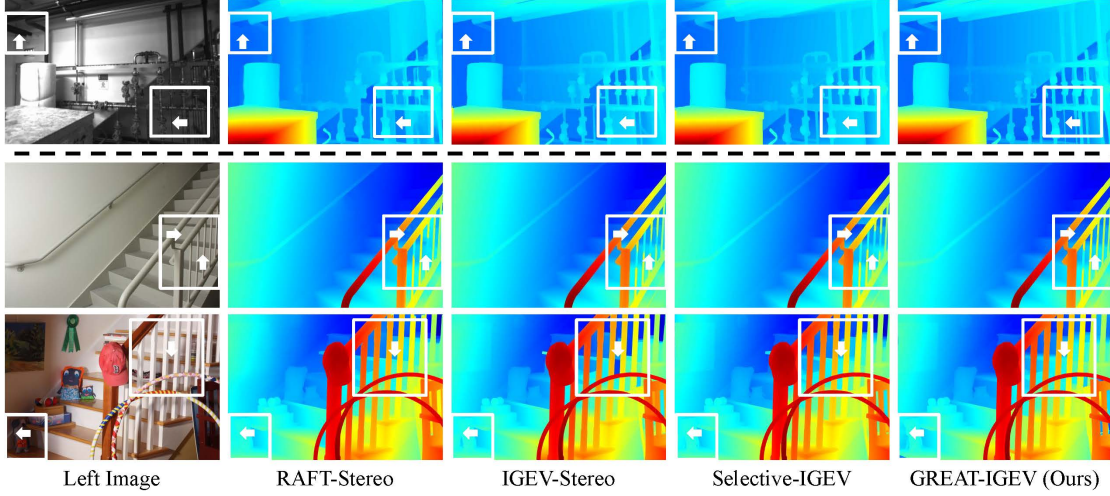


Figure 5. Qualitative results on the ETH3D (**Row 1**) and Middlebury (**Row 2 & 3**) test sets. Our GREAT-IGEV produces clearer and more consistent geometric structures in large textureless and repetitive texture regions, compared to IGEV-Stereo.

Model	ETH3D		Middlebury	
	Bad 0.5	Bad 1.0	Bad 2.0	Bad 4.0
GM-Stereo [47]	5.94	1.83	7.14	2.96
RAFT-Stereo [18]	7.04	2.44	4.74	2.75
CRE-Stereo [17]	3.58	<u>0.98</u>	3.71	2.04
IGEV-Stereo [43]	3.52	<u>1.12</u>	4.83	3.33
Selective-IGEV [37]	3.06	1.23	2.51	1.36
IGEV++ [45]	2.98	1.14	3.23	1.82
GREAT-IGEV (Ours)	2.18	0.72	2.81	1.73

Table 7. Quantitative evaluation on ETH3D and Middlebury benchmarks (**bold**: best; underline: second best).

passes Selective-IGEV [37] by 6.9% on 2-noc metric. On KITTI 2015, our GREAT-IGEV outperforms IGEV-Stereo [43] by 8.1% on Noc-D1-all metric. As shown in Fig. 4, both GREAT-IGEV and GREAT-Selective demonstrate superior performance over their counterparts in occluded and textureless regions.

ETH3D. Following CRE-Stereo [17] and GM-Stereo [47], we use a variety of public stereo datasets for training, with a crop size of 384 x 512 and a batch size of 8. Initially, the Scene Flow pretrained model is fine-tuned on mixed Tartan Air [36], CREStereo [17], Scene Flow [25], Sintel Stereo [3], InStereo2k [2] and ETH3D [29] datasets for 300k steps. Then we fine-tune it on the mixed CREStereo [17], InStereo2k [2] and ETH3D [29] datasets for another 100k steps. As shown in Tab. 7, our GREAT-IGEV ranks first among all published methods, outperforming IGEV-Stereo [43] by 38.1% on Bad 0.5 metric. Moreover, GREAT-IGEV exhibits superior performance in occluded and textureless regions, as illustrated in Fig. 5.

Middlebury. In line with CRE-Stereo [17] and GM-Stereo [47], we first fine-tune the Scene Flow pretrained model on the mixed Tartan Air [36], CREStereo [17], Scene

Flow [25], Falling Things [33], InStereo2k [2], CARLA HR-VS [48] and Middlebury [28] datasets using a crop size of 384 x 512 for 200k steps. Subsequently, we fine-tune it on the mixed CREStereo [17], Falling Things [33], InStereo2k [2], CARLA HR-VS [48] and Middlebury [28] datasets using a crop size of 384 x 768 with a batch size of 8 for another 100k steps. As shown in Tab. 7, our GREAT-IGEV ranks second among all published methods, outperforming IGEV-Stereo [43] by 41.8% on Bad 2.0 metric. Moreover, GREAT-IGEV exhibits superior performance in occluded, textureless, and repetitive texture regions, as illustrated in Fig. 5.

5. Conclusion and Future Work

We introduce GREAT-Stereo, a novel framework compatible with various iterative stereo-matching methods. Integrating Spatial (SA) and Matching (MA) Attention, the network enhances global context from spatial dimensions and epipolar lines. The combination of SA and MA facilitates Volume Attention (VA) which excites the global context within cost volume for a more robust construction. GREAT-Stereo leads in Scene Flow, KITTI, ETH3D, and Middlebury benchmarks. It demonstrates superior capability in leveraging global context to resolve matching ambiguities in ill-posed regions.

On top of our proposed framework, we plan to investigate two extra challenges in the future: 1) MA incurs intensive computational costs with long epipolar lines; 2) Among the ill-posed areas, the reflective ones pose a sub-optimal challenge caused by specular surface lighting conditions rather than lacking global geometric factors, hence requiring an extra module to handle these areas.

Acknowledgement

The work is supported by a grant from Hong Kong Research Grant Council under GRF 11210622.

References

[1] Antyanta Bangunharcana, Jae Won Cho, Seokju Lee, In So Kweon, Kyung-Soo Kim, and Soohyun Kim. Correlate-and-excite: Real-time stereo matching via guided cost volume excitation. In *2021 IEEE/RSJ International Conference on Intelligent Robots and Systems (IROS)*, pages 3542–3548. IEEE, 2021. 5

[2] Wei Bao, Wei Wang, Yuhua Xu, Yulan Guo, Siyu Hong, and Xiaohu Zhang. Instereo2k: a large real dataset for stereo matching in indoor scenes. *Science China Information Sciences*, 63:1–11, 2020. 8

[3] Daniel J Butler, Jonas Wulff, Garrett B Stanley, and Michael J Black. A naturalistic open source movie for optical flow evaluation. In *Computer Vision–ECCV 2012: 12th European Conference on Computer Vision, Florence, Italy, October 7–13, 2012, Proceedings, Part VI 12*, pages 611–625. Springer, 2012. 8

[4] Yohann Cabon, Naila Murray, and Martin Humenberger. Virtual kitti 2. *arXiv preprint arXiv:2001.10773*, 2020. 7

[5] Jia-Ren Chang and Yong-Sheng Chen. Pyramid stereo matching network. In *Proceedings of the IEEE conference on computer vision and pattern recognition*, pages 5410–5418, 2018. 1, 2, 5

[6] Junda Cheng, Xin Yang, Yuechuan Pu, and Peng Guo. Region separable stereo matching. *IEEE Transactions on Multimedia*, 25:4880–4893, 2022.

[7] Junda Cheng, Gangwei Xu, Peng Guo, and Xin Yang. Coatsrnet: Fully exploiting convolution and attention for stereo matching by region separation. *International Journal of Computer Vision*, 132(1):56–73, 2024. 2

[8] Xuelian Cheng, Yiran Zhong, Mehrtash Harandi, Yuchao Dai, Xiaojun Chang, Hongdong Li, Tom Drummond, and Zongyuan Ge. Hierarchical neural architecture search for deep stereo matching. *Advances in neural information processing systems*, 33:22158–22169, 2020. 7

[9] Alexey Dosovitskiy, Lucas Beyer, Alexander Kolesnikov, Dirk Weissenborn, Xiaohua Zhai, Thomas Unterthiner, Mostafa Dehghani, Matthias Minderer, Georg Heigold, Sylvain Gelly, Jakob Uszkoreit, and Neil Houlsby. An image is worth 16x16 words: Transformers for image recognition at scale. *ICLR*, 2021. 4

[10] Andreas Geiger, Philip Lenz, and Raquel Urtasun. Are we ready for autonomous driving? the kitti vision benchmark suite. In *2012 IEEE conference on computer vision and pattern recognition*, pages 3354–3361. IEEE, 2012. 1, 5

[11] Xiaodong Gu, Zhiwen Fan, Siyu Zhu, Zuozhuo Dai, Feitong Tan, and Ping Tan. Cascade cost volume for high-resolution multi-view stereo and stereo matching. In *Proceedings of the IEEE/CVF conference on computer vision and pattern recognition*, pages 2495–2504, 2020. 2

[12] Xiaoyang Guo, Kai Yang, Wukui Yang, Xiaogang Wang, and Hongsheng Li. Group-wise correlation stereo network. In *Proceedings of the IEEE/CVF conference on computer vision and pattern recognition*, pages 3273–3282, 2019. 1, 2, 7

[13] Heiko Hirschmuller. Accurate and efficient stereo processing by semi-global matching and mutual information. In *2005 IEEE computer society conference on computer vision and pattern recognition (CVPR’05)*, pages 807–814. IEEE, 2005. 1

[14] Shihao Jiang, Dylan Campbell, Yao Lu, Hongdong Li, and Richard Hartley. Learning to estimate hidden motions with global motion aggregation. In *Proceedings of the IEEE/CVF international conference on computer vision*, pages 9772–9781, 2021. 2, 3

[15] Junpeng Jing, Jiankun Li, Pengfei Xiong, Jiangyu Liu, Shuaicheng Liu, Yichen Guo, Xin Deng, Mai Xu, Lai Jiang, and Leonid Sigal. Uncertainty guided adaptive warping for robust and efficient stereo matching. In *Proceedings of the IEEE/CVF International Conference on Computer Vision*, pages 3318–3327, 2023. 2

[16] Alex Kendall, Hayk Martirosyan, Saumitro Dasgupta, Peter Henry, Ryan Kennedy, Abraham Bachrach, and Adam Bry. End-to-end learning of geometry and context for deep stereo regression. In *Proceedings of the IEEE international conference on computer vision*, pages 66–75, 2017. 1, 2

[17] Jiankun Li, Peisen Wang, Pengfei Xiong, Tao Cai, Ziwei Yan, Lei Yang, Jiangyu Liu, Haoqiang Fan, and Shuaicheng Liu. Practical stereo matching via cascaded recurrent network with adaptive correlation. In *Proceedings of the IEEE/CVF conference on computer vision and pattern recognition*, pages 16263–16272, 2022. 1, 2, 8

[18] Lahav Lipson, Zachary Teed, and Jia Deng. Raft-stereo: Multilevel recurrent field transforms for stereo matching. In *2021 International Conference on 3D Vision (3DV)*, pages 218–227. IEEE, 2021. 1, 2, 3, 5, 6, 7, 8

[19] Changlin Liu, Linjun Sun, Xin Ning, Jian Xu, Lina Yu, Kajie Zhang, and Weijun Li. Adaptively identify and refine ill-posed regions for accurate stereo matching. *Neural Networks*, 178:106394, 2024. 2

[20] Chuang-Wei Liu, Qijun Chen, and Rui Fan. Playing to vision foundation model’s strengths in stereo matching. *arXiv preprint arXiv:2404.06261*, 2024. 7

[21] Fenglin Liu, Xuancheng Ren, Zhiyuan Zhang, Xu Sun, and Yuexian Zou. Rethinking skip connection with layer normalization in transformers and resnets. *arXiv preprint arXiv:2105.07205*, 2021. 4

[22] Ze Liu, Yutong Lin, Yue Cao, Han Hu, Yixuan Wei, Zheng Zhang, Stephen Lin, and Baining Guo. Swin transformer: Hierarchical vision transformer using shifted windows. In *Proceedings of the IEEE/CVF international conference on computer vision*, pages 10012–10022, 2021. 4

[23] Zihua Liu, Yizhou Li, and Masatoshi Okutomi. Global occlusion-aware transformer for robust stereo matching. In *Proceedings of the IEEE/CVF Winter Conference on Applications of Computer Vision*, pages 3535–3544, 2024. 2, 7

[24] I Loshchilov. Decoupled weight decay regularization. *arXiv preprint arXiv:1711.05101*, 2017. 5

[25] Nikolaus Mayer, Eddy Ilg, Philip Hausser, Philipp Fischer, Daniel Cremers, Alexey Dosovitskiy, and Thomas Brox. A

large dataset to train convolutional networks for disparity, optical flow, and scene flow estimation. In *Proceedings of the IEEE conference on computer vision and pattern recognition*, pages 4040–4048, 2016. 1, 2, 5, 8

[26] Moritz Menze and Andreas Geiger. Object scene flow for autonomous vehicles. In *Proceedings of the IEEE conference on computer vision and pattern recognition*, pages 3061–3070, 2015. 1, 2, 5, 7

[27] Mark Sandler, Andrew Howard, Menglong Zhu, Andrey Zhmoginov, and Liang-Chieh Chen. Mobilenetv2: Inverted residuals and linear bottlenecks. In *Proceedings of the IEEE conference on computer vision and pattern recognition*, pages 4510–4520, 2018. 3

[28] Daniel Scharstein, Heiko Hirschmüller, York Kitajima, Greg Krathwohl, Nera Nešić, Xi Wang, and Porter Westling. High-resolution stereo datasets with subpixel-accurate ground truth. In *Pattern Recognition: 36th German Conference, GCPR 2014, Münster, Germany, September 2-5, 2014, Proceedings 36*, pages 31–42. Springer, 2014. 1, 2, 5, 7, 8

[29] Thomas Schops, Johannes L Schonberger, Silvano Galliani, Torsten Sattler, Konrad Schindler, Marc Pollefeys, and Andreas Geiger. A multi-view stereo benchmark with high-resolution images and multi-camera videos. In *Proceedings of the IEEE conference on computer vision and pattern recognition*, pages 3260–3269, 2017. 1, 2, 5, 7, 8

[30] Zhelun Shen, Yuchao Dai, and Zhibo Rao. Cfnet: Cascade and fused cost volume for robust stereo matching. In *Proceedings of the IEEE/CVF conference on computer vision and pattern recognition*, pages 13906–13915, 2021. 2

[31] Zhelun Shen, Yuchao Dai, Xibin Song, Zhibo Rao, Dingfu Zhou, and Liangjun Zhang. Pcw-net: Pyramid combination and warping cost volume for stereo matching. In *European conference on computer vision*, pages 280–297. Springer, 2022. 2

[32] Leslie N Smith and Nicholay Topin. Super-convergence: Very fast training of neural networks using large learning rates. In *Artificial intelligence and machine learning for multi-domain operations applications*, pages 369–386. SPIE, 2019. 5

[33] Jonathan Tremblay, Thang To, and Stan Birchfield. Falling things: A synthetic dataset for 3d object detection and pose estimation. In *Proceedings of the IEEE Conference on Computer Vision and Pattern Recognition Workshops*, pages 2038–2041, 2018. 8

[34] A Vaswani. Attention is all you need. *Advances in Neural Information Processing Systems*, 2017. 4

[35] Chen Wang, Xiang Wang, Jiawei Zhang, Liang Zhang, Xiao Bai, Xin Ning, Jun Zhou, and Edwin Hancock. Uncertainty estimation for stereo matching based on evidential deep learning. *pattern recognition*, 124:108498, 2022. 2

[36] Wenshan Wang, Delong Zhu, Xiangwei Wang, Yaoyu Hu, Yuheng Qiu, Chen Wang, Yafei Hu, Ashish Kapoor, and Sebastian Scherer. Tartanair: A dataset to push the limits of visual slam. In *2020 IEEE/RSJ International Conference on Intelligent Robots and Systems (IROS)*, pages 4909–4916. IEEE, 2020. 8

[37] Xianqi Wang, Gangwei Xu, Hao Jia, and Xin Yang. Selective-stereo: Adaptive frequency information selection for stereo matching. In *Proceedings of the IEEE/CVF Conference on Computer Vision and Pattern Recognition*, pages 19701–19710, 2024. 2, 3, 4, 6, 7, 8

[38] Yun Wang, Longguang Wang, Kunhong Li, Yongjian Zhang, Dapeng Oliver Wu, and Yulan Guo. Cost volume aggregation in stereo matching revisited: A disparity classification perspective. *IEEE Transactions on Image Processing*, 2024. 1

[39] Yun Wang, Kunhong Li, Longguang Wang, Junjie Hu, Dapeng Oliver Wu, and Yulan Guo. Adstereo: Efficient stereo matching with adaptive downsampling and disparity alignment. *IEEE Transactions on Image Processing*, 2025. 1

[40] Yun Wang, Longguang Wang, Chenghao Zhang, Yongjian Zhang, Zhanjie Zhang, Ao Ma, Chenyou Fan, Tin Lun Lam, and Junjie Hu. Learning robust stereo matching in the wild with selective mixture-of-experts. *arXiv preprint arXiv:2507.04631*, 2025. 2

[41] Yun Wang, Jiahao Zheng, Chenghao Zhang, Zhanjie Zhang, Kunhong Li, Yongjian Zhang, and Junjie Hu. Dualnet: Robust self-supervised stereo matching with pseudo-label supervision. In *Proceedings of the AAAI Conference on Artificial Intelligence*, pages 8178–8186, 2025. 1

[42] Gangwei Xu, Junda Cheng, Peng Guo, and Xin Yang. Attention concatenation volume for accurate and efficient stereo matching. In *Proceedings of the IEEE/CVF conference on computer vision and pattern recognition*, pages 12981–12990, 2022. 1, 2, 7

[43] Gangwei Xu, Xianqi Wang, Xiaohuan Ding, and Xin Yang. Iterative geometry encoding volume for stereo matching. In *Proceedings of the IEEE/CVF Conference on Computer Vision and Pattern Recognition*, pages 21919–21928, 2023. 2, 3, 5, 6, 7, 8

[44] Gangwei Xu, Yun Wang, Junda Cheng, Jinhui Tang, and Xin Yang. Accurate and efficient stereo matching via attention concatenation volume. *IEEE Transactions on Pattern Analysis and Machine Intelligence*, 2023. 1, 2

[45] Gangwei Xu, Xianqi Wang, Zhaoxing Zhang, Junda Cheng, Chunyuan Liao, and Xin Yang. Igev++: Iterative multi-range geometry encoding volumes for stereo matching. *IEEE Transactions on Pattern Analysis and Machine Intelligence*, 2025. 2, 7, 8

[46] Haofei Xu and Juyong Zhang. Aanet: Adaptive aggregation network for efficient stereo matching. In *Proceedings of the IEEE/CVF conference on computer vision and pattern recognition*, pages 1959–1968, 2020. 2

[47] Haofei Xu, Jing Zhang, Jianfei Cai, Hamid Rezatofighi, Fisher Yu, Dacheng Tao, and Andreas Geiger. Unifying flow, stereo and depth estimation. *IEEE Transactions on Pattern Analysis and Machine Intelligence*, 2023. 8

[48] Gengshan Yang, Joshua Manela, Michael Happold, and Deva Ramanan. Hierarchical deep stereo matching on high-resolution images. In *Proceedings of the IEEE/CVF Conference on Computer Vision and Pattern Recognition*, pages 5515–5524, 2019. 8

[49] Zhichao Yin, Trevor Darrell, and Fisher Yu. Hierarchical discrete distribution decomposition for match density estimation. In *Proceedings of the IEEE/CVF conference on*

computer vision and pattern recognition, pages 6044–6053, 2019. [7](#)

[50] Li Yuan, Qibin Hou, Zihang Jiang, Jiashi Feng, and Shuicheng Yan. Volo: Vision outlooker for visual recognition. *IEEE transactions on pattern analysis and machine intelligence*, 45(5):6575–6586, 2022. [4](#)

[51] Jiaxi Zeng, Chengtang Yao, Lidong Yu, Yuwei Wu, and Yunde Jia. Parameterized cost volume for stereo matching. In *Proceedings of the IEEE/CVF International Conference on Computer Vision*, pages 18347–18357, 2023. [1, 2](#)

[52] Feihu Zhang, Victor Prisacariu, Ruigang Yang, and Philip HS Torr. Ga-net: Guided aggregation net for end-to-end stereo matching. In *Proceedings of the IEEE/CVF conference on computer vision and pattern recognition*, pages 185–194, 2019. [2, 7](#)

[53] Feihu Zhang, Xiaojuan Qi, Ruigang Yang, Victor Prisacariu, Benjamin Wah, and Philip Torr. Domain-invariant stereo matching networks. In *Computer Vision–ECCV 2020: 16th European Conference, Glasgow, UK, August 23–28, 2020, Proceedings, Part II 16*, pages 420–439. Springer, 2020. [7](#)

[54] Yongjian Zhang, Longguang Wang, Kunhong Li, Yun Wang, and Yulan Guo. Learning representations from foundation models for domain generalized stereo matching. In *European Conference on Computer Vision*, pages 146–162. Springer, 2024. [2](#)

[55] Haoliang Zhao, Huizhou Zhou, Yongjun Zhang, Jie Chen, Yitong Yang, and Yong Zhao. High-frequency stereo matching network. In *Proceedings of the IEEE/CVF conference on computer vision and pattern recognition*, pages 1327–1336, 2023. [2](#)